Res Chem Intermed (2018) 44:5547–5557
https://doi.org/10.1007/s11164-018-3439-4

Photocatalytic desulfurization of thiophene base on molecular oxygen and zinc phthalocyanine/g-C_3N_4

Gai Zhang[1] · Jingjing Ren[1] · Weifeng Zhao[1] · Min Tian[1] · Weixing Chen[1]

Received: 5 January 2018 / Accepted: 18 April 2018 / Published online: 25 April 2018

Abstract Oxidative desulfurization is considered to be one of the promising new methods for super-deep desulfurization of fuel oil. Herein, zinc phthalocyanine/g-C_3N_4 (g-C_3N_4/ZnTcPc) composites were synthesized by a facile in situ hydrothermal technique, utilizing g-C_3N_4, $Zn(CH_3COO)_2$ and 1,2,4-benzenetricarboxylic anhydride as the precursors. The crystal structure, morphology and chemical environment of the catalysts were respectively confirmed by X-ray diffraction (XRD), transmission electron microscopy (TEM) and X-ray photoelectron spectroscopy (XPS). Photocatalytic activity of the resulting g-C_3N_4/ZnTcPc composites was evaluated by desulfurization of thiophene in fuel under visible light with molecular O_2 as the oxidant. Compared with pure g-C_3N_4 and ZnTcPc, g-C_3N_4/ZnTcPc presented a significantly enhanced photocatalytic activity for the degradation of thiophene in fuel under visible irradiation. Sulfur content of model gasoline (800 ppm) after desulfurization for 90 min was decreased to 125 ppm. The possible preparation pathway of g-C_3N_4/ZnTcPc has been proposed according to the results of XRD and TEM. The formation mechanism of g-C_3N_4/ZnTcPc–O_2 complex is proposed to be desulfurization by molecular oxygen.

Keywords Zinc phthalocyanine/g-C_3N_4 · Molecular oxygen · Desulfurization · Thiophene

✉ Gai Zhang
gaizhang930@126.com

[1] School of Materials Science and Chemical Engineering, Xi'an Technological University, Xi'an 710021, China

Introduction

Deep desulfurization of liquid hydrocarbon fuels has become an important research subject worldwide due to environmental concern. Thiophene, benzothiophene and dibenzothiophene as the main sulfur-containing compounds in crude oil pose severe environmental problems [1]. Removal of thiophene and its alkylated derivatives from fuel is an interesting and significant subject. Oxidative desulfurization (ODS) is considered to be one of the promising new methods for super-deep desulfurization of fuel oil [2–6].

g-C_3N_4 as a novel metal-free polymeric photocatalyst shows outstanding photocatalysis in the degradation of organic pollutants [7–10]. However, the photo-excited band of pure g-C_3N_4 is around 450 nm with a band gap of 2.7 eV, which lies in the UV region [11]. Extensive efforts have been made to improve the practical photoexcited band of g-C_3N_4 [12, 13]. Among these efforts, using dye compounds, especially metal phthalocyanine (MPc) compounds which possess a wide visible light response (600–800 nm), have attracted much interest [14–19]. Therefore, electron transfer from MPc to g-C_3N_4 is more energetically favorable to a higher electron–hole separation, and the photocatalytic activity of MPc-sensitized seems to be extraordinarily vital. Furthermore, MPc compounds are able to photochemically activate triplet oxygen into singlet oxygen ($^1O_2$), which is used as a non-radical oxidant for oxidizing organic pollutants [20]. H_2O_2 is well known among oxidants for ODS. However, the process involves water in the reaction system which results in the biphase problems of the mass transfer and oil phase recovery [21]. Molecular oxygen would be an ideal oxidant for ODS. Molecular oxygen and iron tetranitrophthalocyanine catalyst have been utilized for direct oxidation of dibenzothiophene in hydrocarbon solvent under water-free condition for deep desulfurization [22].

Dipping synthesis is a typical method for MPc-sensitized g-C_3N_4. g-C_3N_4 prepared by thermal decomposition of urea was heat-treated at a high temperature (500 °C) to promote crystallization [23, 24]. However, the thermal analysis shows that the decomposition temperature of metal phthalocyanine is about 300 °C. Recently, a hydrothermal technique has been used extensively for the synthesis of ceramic materials, which takes advantage of direct preparation at low crystallization temperature [25–27]. Here, we show a facile in situ hydrothermal technique developed to synthesize g-C_3N_4/ZnTcPc homogeneous composite, utilizing g-C_3N, $Zn(CH_3COO)_2$ and 1,2,4-benzenetricarboxylic anhydride as precursors. Change in the characteristic absorption peaks of the infrared absorption spectrum and larger changes of the major element binding energy of X-ray photoelectron spectroscopy (XPS) show the existence of π–π stacking interaction in the composites. The photocatalytic activity of g-C_3N_4/ZnTcPc composites was evaluated by the degradation of the thiophene in fuel under visible light with O_2 as the oxidant. The formation mechanism of g-C_3N_4/ZnTcPc–O_2 complex is proposed to be desulfurization by molecular oxygen.

Experimental

Materials

1,2,4-benzenetricarboxylic anhydride (99%) was obtained from Alfa Aesar Co., Ltd. g-C_3N_4 was synthesized according to previous literature [28]. All other reagents were analytical grade and used without further purification.

Characterization

The morphology of the obtained products was characterized by transmission electron microscopy (TEM, JEM-2010). The overall structure of the assemblies was recorded by using a Rigaku (Tokyo, Japan) D/max-2400 X-ray diffractometer with Cu Kα(λ = 0.15406 nm) radiation. The patterns were compared with JCPDS reference data for phase identification. The structures of the products were further determined by Fourier transform infrared (FT-IR) absorbance spectrum analysis on a Bruker Equinox 55 spectrometer (KBr pellets) in the 4000–400-cm^{-1} range. The optical absorption properties were investigate using an UV–Vis spectrometer (UV-2550, Shimadzu). XPS spectra were recorded on a Kratos AXIS ULTRA spectrometer with a monochromated Al Kα X-ray source (1486.6 eV). The C1s peak at 284.5 eV was regarded as the reference point of binding energies. The desulfurization device includes a stainless box vessel, a 400-W halogen HQI-BT 400D lamp (OSRAM, made by SIEMENS Company in Germany) and a 200-ml beaker. Thiophene concentration in fuel was recorded by using an Agilent 6890 gas chromatography spectrometer with a flame photometric detector (FPD).

Preparation of g-C_3N_4

g-C_3N_4 sample was prepared by the thermal decomposition of melamine. White melamine powder was placed into an alumina crucible and heated in air atmosphere at 550 °C for 4 h (the heating rate was 2.3 °C/min). After cooling, the pale-yellow g-C_3N_4 product was collected.

Preparation of g-C_3N_4/ZnTcPc

The g-C_3N_4/ZnTcPc composites were synthesized by a facile in situ hydrothermal technique utilizing g-C_3N_4, $Zn(CH_3COO)_2$ and 1,2,4-benzenetricarboxylic anhydride as the precursors. The weight ratio of ZnTcPc in g-C_3N_4-to-ZnTcPc compositions was 8%. The mixture was poured into a Teflon-lined autoclave and put inside the furnace for preparation at 200 °C through temperature-programming method. The reaction was completed by heating the autoclave to 200 °C and maintaining the temperature for 6 h. All the samples were recovered by washing with deionized water followed by centrifugation for three times and dried at 100 °C in an oven overnight.

In the control tests, the pure particles of ZnTcPc were prepared under the same conditions used for preparing g-C_3N_4/ZnTcPc composites.

Evaluation of photocatalytic activity

The photocatalytic desulfurization experiments were carried out in a 100-mL three-neck flask connected with an oxygen cylinder, a magnetic stirrer and a reflux condenser. The appropriate amount (20 mg) of catalysts was added to a fresh n-octane solution of thiophene (100 mL, 800 μL L^{-1}) and molecular oxygen was bubbled through the reaction solution. Samples (2 mL) were collected every 30 min from the glass flask and analyzed to determine sulfur concentration. Prior to analysis, samples were centrifuged to remove catalyst particles. The residue concentration of thiophene in n-octane and the corresponding sulfone of thiophene in the eluent extracted with dichloromethane were analyzed via an Agilent 6890 gas chromatograph equipped with a capillary column (hp-5, 30 × 0.2 × 0.5 mm) and flame photometric detector. The efficiency of the degradation was calculated with the formula $D\ (\%) = (C_0 - C)/C_0 \times 100\%$, in which C_0 and C are the original thiophene concentration after the adsorption/desorption equilibrium and the residual thiophene concentration after the degradation, respectively.

Results and discussion

UV–Vis and FT-IR spectra

As shown in Fig. 1, the UV–Vis spectrum of ZnTcPc shows two peaks, one Q band peak at 620 and 670 nm, representing the characteristic bands of the dimer and monomer of ZnTcPc, respectively. The Q band activity was mainly attributed to the

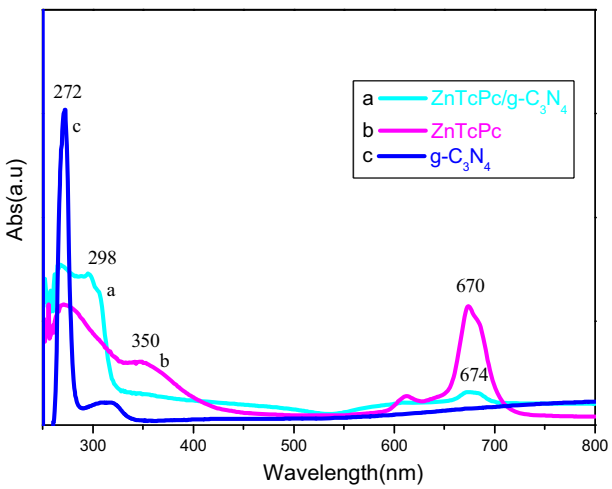

Fig. 1 UV-Vis pattern of g-C_3N_4, g-C_3N_4/ZnTcPc and ZnTcPc

monomer. Compared with the ZnTcPc, the absorption of g-C_3N_4/ZnTcPc samples are slightly red-shifted from 670 to 674 nm, which is related to π–π stacking interaction in the composites. Moreover, a shoulder peak at about 620 nm disappeared, indicating that the phthalocyanine aggregation was significantly reduced.

Figure 2 shows the FT-IR spectra of the pure g-C_3N_4, ZnTcPc and g-C_3N_4/ZnTcPc. The characteristic vibration peaks assigned to typical g-C_3N_4 indicated the successful preparation of the g-C_3N_4. The peaks at 1200–1600 cm^{-1} are attributed to the stretching vibrations of C–N heterocycles. The appearance at 808 cm^{-1} is assigned to the characteristic breathing modes of triazine units [29]. The bands at 730, 907, 945, 1011, 1132, 1287 and 1711 cm^{-1} are assigned to typical the characteristic peaks of ZnTcPc [30]. The FT-IR spectra of g-C_3N_4/ZnTcPc samples indicated the formation of ZnTcPc on the surface of g-C_3N_4.

XRD spectra of g-C_3N_4/ZnTcPc

The XRD pattern of the highly graphitic-like structures for g-C_3N_4 samples are shown in Fig. 3. The characteristic inter-layer stacking (002) peak at 27.6° suggests the formation of a well-developed C_3N_4 layer structure. Additionally, it should be noteworthy that an in-planar peak at 13.1° for g-C_3N_4 samples related to an interplanar separation of 0.682 nm can be observed [31]. The peak at 13.1° is indexed as (100) in JCPDS 87-1526 [32]. The XRD spectrum indicates that pure ZnTcPc is completely amorphous. However, with the ZnTcPc formatted on the surface of g-C_3N_4, the typical peaks of ZnTcPc at 6.2° and 25.7° are detected from XRD pattern for g-C_3N_4/ZnTcPc samples. Compared with the native g-C_3N_4 from melamine, the XRD peaks of g-C_3N_4/ZnTcPc samples are slightly shifted to a lower angle, which is related to the formation of a ZnTcPc framework. More significantly, due to the formation of ZnTcPc, the new peaks at 9.4 ° and 16.7 ° of g-C_3N_4/ZnTcPc

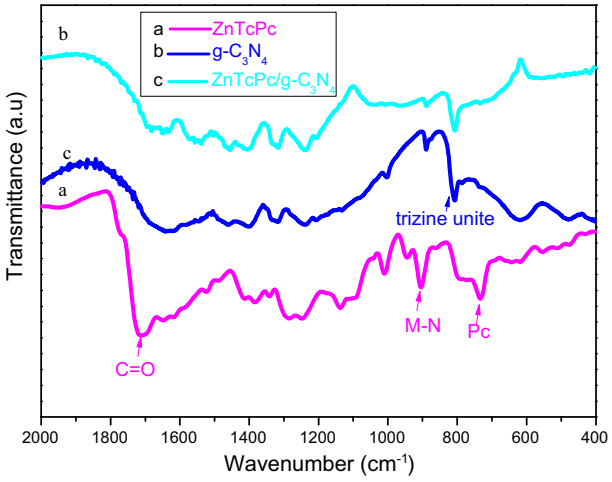

Fig. 2 FT-IR pattern of g-C_3N_4, g-C_3N_4/ZnTcPc and ZnTcPc

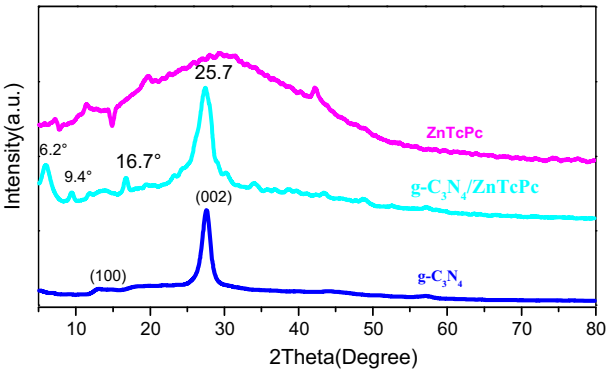

Fig. 3 XRD pattern of g-C_3N_4, g-C_3N_4/ZnTcPc and ZnTcPc composites

are observed, demonstrating that weakening the π-π stacking interaction of ZnTcPc and g-C_3N_4 has an effect on the structure of g-C_3N_4/ZnTcPc. It can be concluded that the diffraction peaks belonging to g-C_3N_4 in the composites are intact, showing that the introduction of ZnTcPc does not change the graphitic structures of pristine samples.

XPS spectra of g-C_3N_4/ZnTcPc

XPS measurements were performed to investigate the surface composition and chemical state of various species. Figure 4 shows the C1s, N1s and Zn2p high-resolution XPS spectra of g-C_3N_4 and g-C_3N_4/ZnTcPc composite. For pure g-C_3N_4,

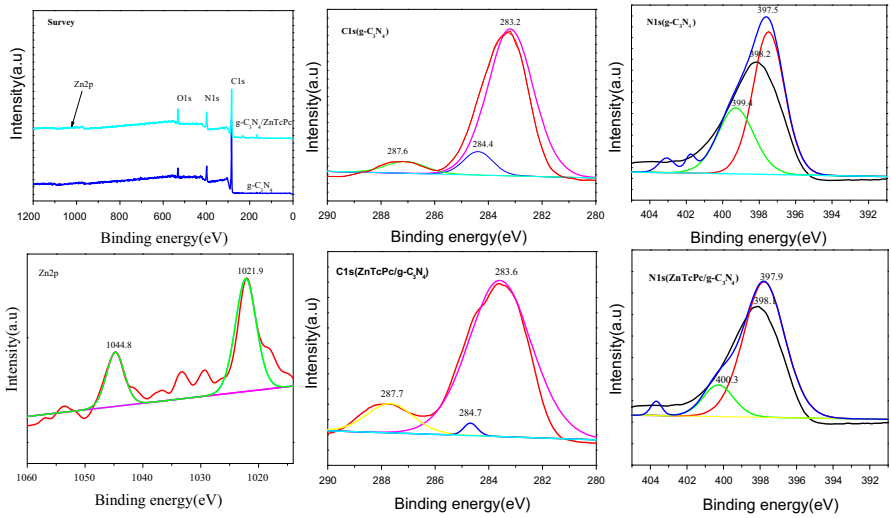

Fig. 4 High-resolution XPS spectra survey of C1s and N1s obtained in g-C_3N_4 and g-C_3N_4/ZnTcPc composite

the C1s peaks located at 284.4 and 287.6 eV could be attributed to sp^2C and a N–C–N bond, respectively [33]. Meanwhile, for g-C_3N_4/ZnTcPc, the three peaks correspond to sp^2C (284.7 eV), C–COOH (283.6 eV) and N–C–N (287.7 eV), respectively. According to the N1s peak of ZnTcPc/g-C_3N_4, the observed electron binding energy value is 397.9 eV, corresponding to the triazine rings. Meanwhile, the N1s peak at 398.1 eV is attributed to aza bridging and pyrrole nitrogen atoms [34]. The weak peak at 399.4 eV indicates the presence of the tertiary nitrogen N–$(C)_3$ groups of g-C_3N_4. The electron binding energy value of amino functions (C–N–H) is observed at 400.2 eV [35]. Zn 2p3/2 and Zn 2p1/2 peaks of g-C_3N_4/ZnTcPc are observed at 1021.9 and 1044.8 eV, respectively, while for pure ZnTcPc, the binding energy of Zn 2p is slightly higher than that of g-C_3N_4/ZnTcPc, which could be ascribed to the interactions between the g-C_3N_4 support and ZnTcPc particle. That is a consequence of spin–orbit coupling with the electron-rich surface of g-C_3N_4 and an unoccupied Zn orbital.

TEM spectra of g-C_3N_4/ZnTcPc

The TEM images of g-C_3N_4 and g-C_3N_4/ZnTcPc composites are shown in Fig. 5. Compared to the pure g-C_3N_4 sample, ZnTcPc is well dispersed on the external surface of g-C_3N_4 because the g-C_3N_4 with high surface area can prevent the aggregation of ZnTcPc during the preparation of the composite. The good distribution and coverage of ZnTcPc on the g-C_3N_4 is expected to enhance the photocatalytic performance of the g-C_3N_4/ZnTcPc nanocomposites.

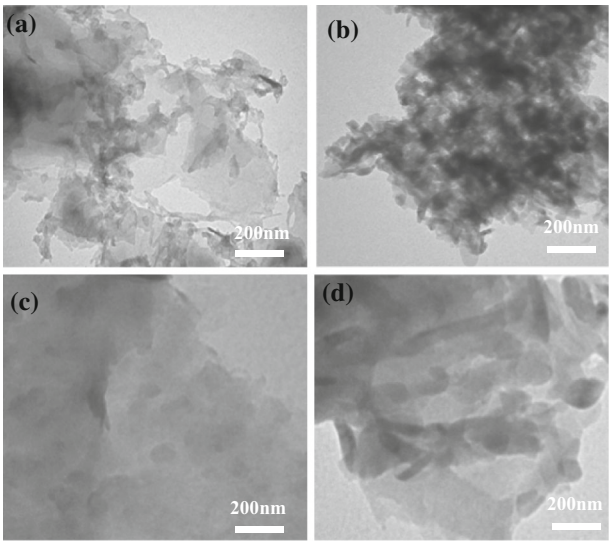

Fig. 5 **a** TEM images of g-C_3N_4 (× 100,000), **b** g-C_3N_4/ZnTcPc (1%mol, × 100,000), **c** g-C_3N_4 (× 150,000) and **d** g-C_3N_4/ZnTcPc (1%mol, × 150,000) composites

Mechanism of the formation of g-C_3N_4/ZnTcPc

The proposed formation mechanism of g-C_3N_4/ZnTcPc composites synthesized by in situ hydrothermal technique is as follows (Fig. 6). The Zn^{2+} and 1,2,4-benzenetricarboxylic anhydride molecules were dispersed homogeneously on the surface to reduce the surface energy of g-C_3N_4. The Zn^{2+} and 1,2,4-benzenetricarboxylic anhydride molecules then undergo a reorganization and recrystallization process during the hydrothermal process. The physical absorption effect limited the long-distance movement of the metal phthalocyanine molecules and reduced the collision with other molecules in farther distances. The phthalocyanine aggregation was significantly reduced. The metal phthalocyanine molecules formatted on the particle surfaces of g-C_3N_4. π–π interaction between phthalocyanine ZnTcPc and the g-C_3N_4 surface was in favor of the electron transfer process from the excited phthalocyanine to the conduction band of the g-C_3N_4 [36].

Photocatalytic efficiency of g-C_3N_4/ZnTcPc

The photocatalytic activities of the as-prepared g-C_3N_4, ZnTcPc and g-C_3N_4/ZnTcPc were evaluated by the degradation of thiophene in fuel under visible light irradiation. The photocatalytic activities of blank, g-C_3N_4, ZnTcPc and g-C_3N_4/ZnTcPc were 6.97, 59.30, 54.3 and 84.42% after degradation for 90 min, respectively (Fig. 7). The photocatalytic activity of the g-C_3N_4/ZnTcPc was obviously improved 15.12% compared with that of g-C_3N_4 under visible light irradiation. The high photocatalytic activity of the samples is due to the electron transfer process from the excited phthalocyanine to the g-C_3N_4. The dye-sensitized g-C_3N_4 makes the light absorption extend to the visible spectral region. In addition, the uniform dispersion of the ZnTcPc in g-C_3N_4 particles also contributes to the higher photocatalytic efficiency of the g-C_3N_4/ZnTcPc composite. The photocatalytic desulfurization rate of the sensitized g-C_3N_4/ZnTcPc composite reaches 84.42%. Treatment with superoxide radicals converted the thiophene to a sulfuric acid radical ion and sulfone. To evaluate the stability of the g-C_3N_4/ZnTcPc catalysts, samples were separated from the suspension after photocatalytic degradation reaction for 90 min, and then collected by centrifugation and dried at 80 °C. The recovered photocatalysts were reused for subsequent photocatalytic reaction under the same conditions. The degradation rate decreased to 81%. The

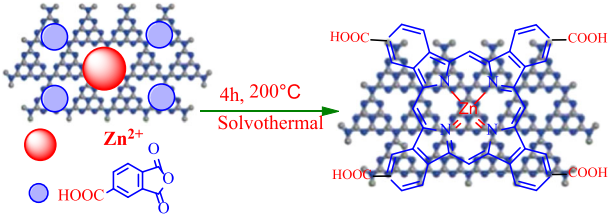

Fig. 6 The proposed formation mechanism of g-C_3N_4/ZnTcPc composites

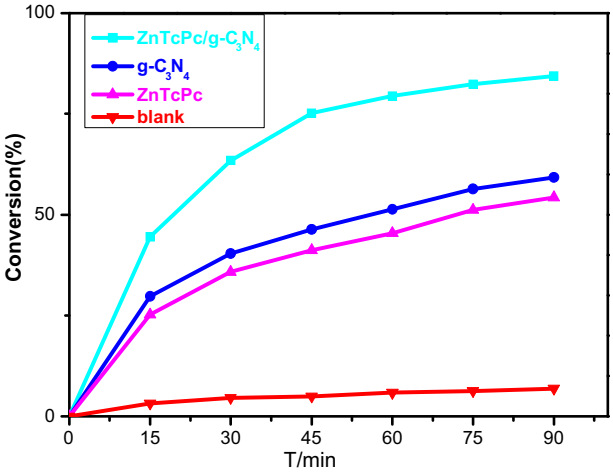

Fig. 7 The photocatalytic desulfurization rate of g-C_3N_4, g-C_3N_4/ZnTcPc and ZnTcPc composite

results indicate that zinc phthalocyanine still wrapped on the g-C_3N_4 carrier during the reaction.

Photocatalytic degradation mechanism of ZnTcPc/g-C_3N_4

Based on our experimental results and reported literature, a mechanism was proposed for the photocatalytic activity of g-C_3N_4 and g-C_3N_4/ZnTcPc catalysts in the degradation of thiophene in fuel as follows: first, molecular oxygen was bubbled through the reaction solution and adsorbed on the surface of g-C_3N_4/ZnTcPc. What is more, the dissolved oxygen molecule adsorption and bonding on the metal phthalocyanine was proposed to be the formation of the g-C_3N_4/ZnTcPc-O_2 complex. ZnTcPc molecular was stimulated by the light source to produce electron–hole pairs in the photocatalytic degradation process of thiophene in fuel. O_2-ZnTcPc is immediately converted to $^{*}O_2$-ZnTcPc^{+}, which is capable of degrading thiophene. At the same time, since the lowest unoccupied molecular orbital (LUMO) of ZnTcPc is higher than the conduction band (CB) of g-C_3N_4, the excited electron on ZnTcPc could be easily injected into g-C_3N_4, which makes charge separation more efficient and reduces the probability of recombination (Fig. 8). The photogenerated electrons on the CB of g-C_3N_4 can further react with dissolved oxygen to form $\cdot O^{2-}$, which converts thiophene to a sulfuric acid radical ion and sulfone [39]. The quantum yield of the photocatalytic redox process increases as a result of the additional formation of $^{*}O_2$-ZnTcPc^{+} and $\cdot O^{2-}$ on g-C_3N_4/ZnTcPc-O_2 [37, 38].

The thiophene was converted to a sulfuric acid radical ion and sulfone by $^{*}O_2$-ZnTcPc^{+} and $\cdot O^{2-}$. The residue concentration of the corresponding sulfone of thiophene in the eluent extracted with dichloromethane was analyzed using the Agilent 6890 gas chromatograph. In order to detect the product SO_4^{2-}, the $Ba(OH)_2$

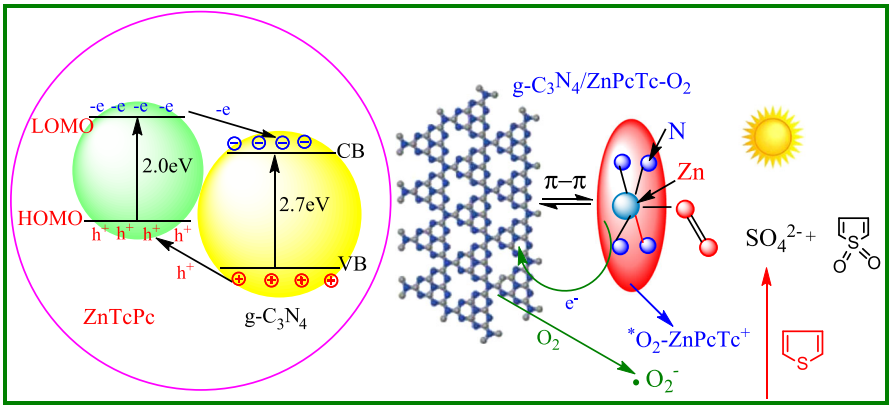

Fig. 8 Photocatalytic degradation mechanism of g-C_3N_4/ZnTcPc

solution was added into the resulting water phase, which made precipitates with the SO_4^{2-} ion [39].

$$\mathrm{ZnTcPc/C_3N_4} + h\nu \rightarrow \mathrm{ZnTcPc/C_3N_4}\left(h_{\mathrm{VB}}^{+}\right) + \mathrm{ZnTcPc/C_3N_4}\left(e_{\mathrm{CB}}^{-}\right)$$

$$\mathrm{C_4H_4S} + \mathrm{ZnTcPc/C_3N_4}\left(h_{\mathrm{VB}}^{+}\right) \rightarrow \mathrm{C_4H_4S^{+}\cdot}$$

$$\mathrm{O_2} + \mathrm{ZnTcPc/C_3N_4}\left(e_{\mathrm{CB}}^{-}\right) \rightarrow \cdot\mathrm{O_2^{-}}$$

$$\mathrm{C_4H_4S^{+}\cdot} + \cdot\mathrm{O_2^{-}} \rightarrow \mathrm{C_4H_4SO_2(sulphone)}$$

$$\mathrm{C_4H_4SO_2} + \cdot\mathrm{O_2^{-}} \rightarrow \mathrm{SO_3}$$

$$\mathrm{SO_3} + \mathrm{Ba(OH)_2} = \mathrm{BaSO_4}(\downarrow)$$

Conclusions

The g-C_3N_4/ZnTcPc composites synthesized by an in situ hydrothermal technique preserved better dispersion and visible light response. The changing characteristic absorption peaks of the UV–Vis absorption spectrum and larger changes of the major element binding energy as per XPS show the presence of strong π–π interaction in the composites. π–π interaction between phthalocyanine ZnTcPc and the g-C_3N_4 surface is in favor of the electron transfer process and reducing the phthalocyanine aggregation. Adsorption and bonding of oxygen molecules on the metal phthalocyanine are proposed as the mechanism of formation of the g-C_3N_4/ZnTcPc-O_2 complex, which is beneficial for formation of the oxygen-free radicals ($^{*}O_2$-ZnTcPc^{+} and $\cdot O^{2-}$). The photocatalytic degradation desulfurization rate of the sensitized g-C_3N_4/ZnTcPc composite reaches 84.42%. The thiophene was converted to a sulfuric acid radical ion and sulfone by $^{*}O_2$-ZnTcPc^{+} and $\cdot O^{2-}$ radicals.

Acknowledgements We gratefully acknowledge financial support of this work by the National Natural Science Foundation of China (Nos. 21501139 and 61604120), and the President Foundation of Xi'an Technological University (XAGDXJJ1611).

References

1. S. Peng, G. Jin, L. Li, K. Li, M. Srinivasan, S. Ramakrishna, J. Chen, Chem. Soc. Rev. **45**, 1225 (2016)
2. C. Wang, Z. Chen, W. Zhu, P. Wu, W. Jiang, Energy Fuel **31**, 1376 (2017)
3. W.S. Zhu, C. Wang, H.P. Li, P.W. Wu et al., Green Chem. **17**, 2464 (2015)
4. C. Wang, W. Zhu, Y. Xu, H. Xu, M. Zhang, Ceram. Int. **40**, 11627 (2014)
5. S. Xun, W. Zhu, Y. Chang, H. Li, M. Zhang, Chem. Eng. J. **288**, 608 (2016)
6. C.A. Martínez, M.A. Rodrigo, I. Sires, O. Scialdone, Chem. Soc. Rev. **115**, 13362 (2015)
7. X. Dai, M. Xie, S. Meng, X. Fu, S. Chen, Appl. Catal. B: Environ. **158–159**, 382 (2014)
8. X. Wang, K. Maeda, A. Thomas, K. Takanabe, G. Xin, J.M. Carlsson, K. Domen, M. Antonietti, Nat. Mater. **8**, 76 (2009)
9. S. Yan, S. Lv, Z. Li, Z. Zou, Dalton Trans. **39**, 1488 (2010)
10. Y. Wang, J. Yao, H. Li, D. Su, M. Antonietti, J. Am. Chem. Soc. **133**, 1022 (2011)
11. S. Zhang, J. Li, M. Zeng, G. Zhao, J. Xu, W. Hu, X. Wang, ACS Appl. Mater. **181**, 169 (2016)
12. W.J. Ong, L.L. Tan, Y.H. Ng, S.T. Yong, S.P. Chai, Chem. Rev. **116**, 7159 (2016)
13. T. Xiong, W.L. Cen, Y.X. Zhang, F. Dong, ACS Catal. **6**, 2462 (2016)
14. X. Chen, X.M. Hu, L. An, Electrocatalysis **5**, 68 (2014)
15. Y.C. Kim, T.Y. Yang, N.J. Jeon, J. Im, S. Jang, T.J. Shin, H.-W. Shin, S. Kim, E. Lee, S. Kim, J.H. Noh, S.I. Seok, J. Seo, Energy Environ. Sci. **10**, 2109 (2017)
16. X.Q. Chen, D.D. Ma, K.C. Cai, J. Coord. Chem. **68**, 732 (2015)
17. W.I. Lin, M.F. Gholami, P. Beyer, N. Severin, F. Shao, R. Zenobi, J.P. Rabe, Chem. Commun. **53**, 724 (2017)
18. H. Lu, N. Kobayashi, Chem. Rev. **116**, 6184 (2016)
19. M. Atzori, L. Tesi, E. Morra, M. Chiesa, L. Sorace, R. Sessoli, J. Am. Chem. Soc. **138**, 2154 (2016)
20. S. Chen, W. Lu, Y. Yao et al., React. Kinet. Mech. Catal. **111**, 535 (2014)
21. S.W. Li, Y.Y. Li, F. Yang, Z. Liu, R.M. Gao, J.S. Zhao, J. Colloid. Interf. Sci. **460**, 8 (2015)
22. J. Zhang, J. Li, T. Ren, Rsc Advances. **4**, 3206 (2014)
23. M. Groenewolt, M. Antonietti, Adv. Mater. **17**, 1789 (2010)
24. L. Huang, H. Xu, Y. Li, H. Li, X. Cheng, Dalton Trans. **42**, 8606 (2013)
25. D.S. Kim, S.Y. Kwak, Appl. Catal. **323**, 110 (2007)
26. H. Yan, X.H. Zhang, J.M. Wu, Powder Technol. **188**, 128 (2008)
27. B. Bayati, A.A. Babaluo, R. Karimi, J. Eur. Ceram. Soc. **28**, 2653 (2008)
28. F. Dong, L. Wu, Y. Sun, M. Fu, Z. Wu, S.C. Lee, J. Mater. Chem. **21**, 15171 (2011)
29. Y.Z. Hong, Y.H. Jiang, C.S. Li, W.Q. Fan, X. Yan, M. Yan, W.D. Shi, Appl. Catal. B **180**, 663 (2016)
30. M.N. Yarasir, M. Kandaz, B.F. Senkal, Polyhedron **26**, 5235 (2007)
31. G.G. Zhang, J.S. Zhang, M.W. Zhang, X.C. Wang, J. Mater. Chem. **22**, 8083 (2012)
32. Y. Wang, J. Yao, H. Li, D. Su, M. Antonietti, J. Am. Chem. Soc. **133**, 2362 (2011)
33. J. Zhang, M. Zhang, C. Yang, X. Wang, Adv. Mater. **26**, 805 (2014)
34. L.J. Yu, X.H. Zhang, C.S. Zhang, L. Lin, R.J. Li, T.Y. Peng, Phys. Chem. Chem. Phys. **16**, 4106 (2014)
35. J.W. Fang, H.Q. Fan, M.M. Li, C.B. Long, J. Mater. Chem. A. **3**, 13819 (2015)
36. T.F. Xu, D.J. Ni, X. Chen, F. Wu, P.F. Ge, W.Y. Lu, H.G. Hu, Z.X. Zhu, W.X. Chen, J. Hazar. Mater. **317**, 17 (2016)
37. W.Y. Lu, T.F. Xu, Y. Wang, H.G. Hu, N. Li, X.M. Jiang, W.X. Chen, Appl. Catal. B: Environ. **180**, 20 (2016)
38. Q. Liang, M. Zhang, C.H. Liu, S. Xu, Z.Y. Li, Appl. Catal. **519**, 107 (2016)
39. N. Zhao, S.W. Li, J.Y. Wang, R.L. Zhang, R.M. Gao, J.S. Zhao, J.L. Wang, J. Solid State Chem. **225**, 347 (2015)